KONA Powder and Particle Journal

KONA Powder and Particle Journal No. 42 (2025) 268–284/https://doi.org/10.14356/kona.2025018 Original Research Paper

Decoding Attractive Interactions in Granular Materials through Vibration-Induced Densification †

Maria-Graciela Cares-Pacheco * and Véronique Falk

Reactions and Chemical Engineering Laboratory (LRGP-CNRS), Université de Lorraine, France

Within the intricate world of granular materials, the behavior of grain assemblies presents complexities characterized by nonlinear and inelastic phenomena, which seamlessly link the microscopic grain scale to the macroscopic bulk scale. A key challenge in understanding the mechanics of granular materials lies in establishing connections between these microscopic grain properties and their macroscopic flow behavior. This study delves into vibration-induced densification, a phenomenon relevant across various technological domains in powder processing and manufacturing. Specifically, we explore the vibrational conditions that induce compaction and decompaction under vertical vibration, employing a particle damper across industrial powders, including glass beads, joint filler, wheat flour, and pharmaceutical excipients. The experiments involve controlling the vibration wave by adjusting parameters such as frequency and amplitude while measuring and recording the acceleration and force signals. Our findings reveal a significant correlation between the force required to decompact the powder bed and the attractive forces between grains. This correlation facilitates the determination of a dimensionless granular number A_d, offering insights into the contact force network at a macroscopic level and its relation to flow indices. By proposing this experimental approach, we provide a straightforward method to unveil the intricate relationship between local particle interactions and the overarching mechanical behavior of granular materials, contributing to advancements in understanding and predicting powder flow behavior.

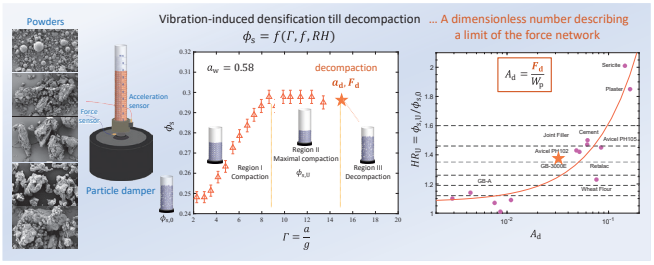

Keywords: densification, compaction, vibration, adhesion, force network

1. Introduction

Throughout history, granular materials such as sand, wheat, and wood have played fundamental roles in human civilization. From ancient times to this day, these materials have been integral to various aspects of daily life and industrial processes. Since the advent of the industrial revolution in the eighteenth century, engineers have grappled with the intricate challenges posed by the handling and processing of grains, many of which revolve around flow-related issues (Bérut et al., 2019; Carson et al., 2019; Ghadiri et al., 2020). Poor flow properties can trigger a cascade of complications, from segregation and feeder blockages to the formation of ratholes, necessitating manual interventions such as hammering and scraping to silos collapsing during storage (Carson et al., 2019; Schulze, 2021).

The behavior of granular assemblies is inherently complex, marked by nonlinear, inelastic effects and highly dissipative interactions that occur across scales—from microscopic grain interactions to macroscopic flow dynamics (Andreotti et al., 2011; Herrmann et al., 1998; Jaeger et al., 1996). This intricate interplay between local particle interactions and global mechanical behavior highlights the necessity for comprehensive, multi-scale research to fully understand granular materials.

The macroscopic mechanical properties of granular materials are intricately linked to the microscale, specifically the particle scale. Unlike elastic solids, which support external forces under loading, granular materials transmit these forces through a percolating network of particles, forming chain-like structures that act as preferential pathways for force transmission (Majmudar and Behringer, 2005; Radjai et al., 2010). The distribution of forces within granular materials is broad and highly heterogeneous. Extensive experimental and numerical research has been conducted to investigate the evolution, properties, and statistical behavior of these force distributions within highly idealized granular assemblies (Kollmer and Daniels, 2019; Papadopoulos et al., 2018; Wu and Wang, 2022). Although force transmission in idealized granular materials presents relatively straightforward dynamics, the force transmission encountered in industrial processing is far more complex. Irregular particle shapes and adhesive interactions complicate the establishment of a direct correspondence between macroscopic and microscopic features, as commonly observed in non-cohesive, circular-shaped granular

† Received 17 May 2024; Accepted 28 August 2024
J-STAGE Advance published online 19 October 2024
* Corresponding author: Maria-Graciela Cares-Pacheco;
Add: Nancy F-54000, France
E-mail: maria-graciela.cares@univ-lorraine.fr
TEL: +33-372-74-7237-49

assemblies (Gilabert et al., 2007; Marteau and Andrade, 2021; Saint-Cyr et al., 2013).

This work aims to address some of these issues by experimentally extracting force network information. The challenge lies in describing an infinite number of packing configurations that seem to statistically retain consistent macroscopic properties. Given this challenge, dynamic densification experiments emerge as a promising approach. The compaction of fine granular materials is a common unit operation across various industries, including pharmaceuticals, cosmetics, metallurgy, agro-food, nuclear, and automotive. It is employed to create products such as agglomerates, capsules, tablets, pellets, and battery electrodes, all of which are designed with specific compositions, porosities, shapes, and strengths. Additionally, compaction can occur as a result of discrete taps or vibrations during transportation or handling. These actions can significantly alter the volume and may lead to the segregation of granular materials. The resulting contact network and force transmission are essential aspects that evolve throughout the compaction process.

When a powder is shaken, the grains reorganize themselves into a denser structure. Several empirical or heuristic models have described the dynamics of compaction under gentle tapping, mainly using glass beads (Knight et al., 1995; Ribière et al., 2005, 2007; Suaza-Montalvo et al., 2023a). The density, or packing fraction, plots depend on the amplitude of the taps and the geometry and are usually described as logarithmically slow. However, the densification of complex (or heterogeneous) granular materials, such as powders, often fails to describe many phenomena encountered during vibration. Whether particles reorganize during densification depends on the energy or force supplied to the powder—the confinement strategy—and is therefore device-related (Saker et al., 2019). The force-wave signal transmitted to the powder bed significantly affects force transmission and densification dynamics (Suaza-Montalvo et al., 2023a).

For instance, in uniaxial compression devices, a step-like force signal is applied to the powder (**Fig. 1A**). At low compression forces, where little to no particle deformation occurs, densification takes place through particle rearrangement as particles roll into void spaces (Cares-Pacheco et al., 2021). In vibration-induced densification, such as in tapping devices like the Densitap, the shock wave generated by rotating a snail cam (**Fig. 1B**) facilitates particle separation and lift-off, creating new pathways for rearrangement (Cares-Pacheco et al., 2021). When utilizing particle dampers (**Fig. 1C**), the transmitted signal to the powder (frequency, amplitude, and period) can be precisely controlled. This control allows for varying porosity levels to be achieved through particle rolling or lift-off, with the latter exhibiting different fluidization regimes (Suaza-Montalvo et al., 2023a). At a fixed frequency, increasing the acceleration is akin to increasing the superficial gas velocity in fluidized beds, leading to different flow regimes ranging from bubbling to slugging to turbulent.

By employing an experimental methodology centered around vibration-induced densification across a spectrum of industrial powders, we aim to explore the mechanics governing force transmission, particle interactions, and densification dynamics. Specifically, our methodology focuses on tracking the evolution of the packing fraction until the powder bed undergoes decompaction or fluidization. This investigation examines the effects of signal frequency and amplitude, powder-column height, and air humidity conditioning.

Our study marks a significant step forward in our ongoing efforts to gain deeper insights into the complexities inherent in granular materials. Of particular interest is the extraction of a dimensionless parameter representing force chains and its correlation with flow indicators.

2. Materials and methods

2.1 Powders

In this study, six powders were selected to represent a wide range of industries and physical characteristics, based on their industrial applications. Two pharmaceutical excipients were chosen: RetaLac®, a binder produced by Meggle for direct compression and dry granulation of modified release formulations, and Avicel® PH-102, a microcrystalline cellulose from FMC Biopolymer®. Avicel® PH-102 is

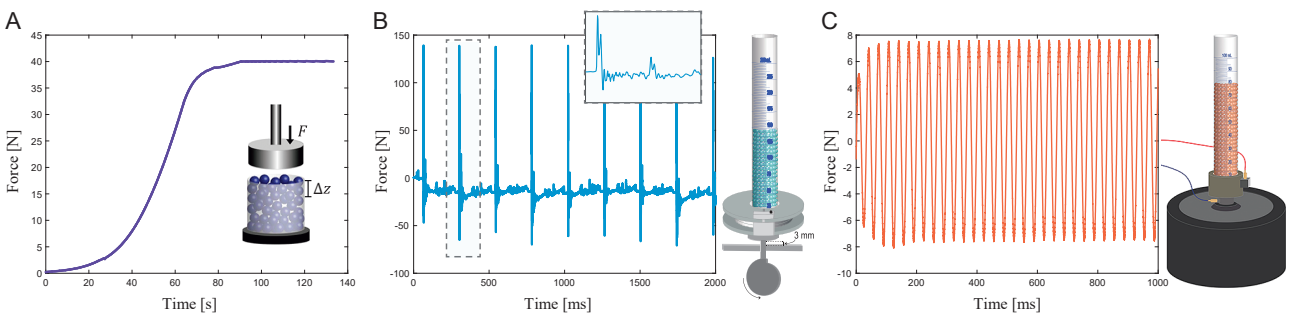

Fig. 1 Schematic representation of various devices used for compacting granular materials, along with the force signal transmitted to the sample. **A)** Uniaxial compression; **B)** Tapping; and **C)** Particle damper.

widely used across various industries as a texturizer, anti-caking agent, fat substitute, emulsifier, extender, and bulking agent in food production. To investigate the effects of highly uniform water-inert materials, two types of glass beads (GB) were selected. Glass beads are often used as "model materials" in granular physics due to their spherical, smooth, and hard particle properties. The first type, GB-A, is monodisperse, while GB 3000E from Potters® Industries LLC (Spheriglass® 135 3000-E), a polydisperse material, is specifically used in highway safety marking. Both types of glass beads were carefully washed prior to use. From the food industry, artisan-made T45 wheat flour from the Poinsignon flour mill in France was selected. Finally, joint filler from MAPEI®, used for grouting tiles and finishing walls, was chosen to represent the construction industry.

The behaviors of these powders in relation to water is presented in **Fig. 2**. The sorption isotherms indicated that the wheat flour (B) absorbed the most water, followed by Avicel PH102 (A) and RetaLac (E). Joint filler (C) exhibited minimal water absorption, while both types of glass beads, 3000E and GB-A (D), remained chemically inert to water. All powders were conditioned and stored at room temperature in sealed containers, with relative humidity maintained at approximately 20 % (using lithium chloride - LiCl) and 60 % (using sodium chloride - NaCl) through saturated salt/water solutions. The samples were allowed to equilibrate until they either matched the environmental conditions or exhibited stable behavior over a week, as confirmed by daily measurements of water activity (a_w) using an Aqualab 4TE from METER.

Details on the microstructural attributes of the powders are illustrated in **Fig. 3**, and their physical properties are summarized in **Table 1**. These properties include the characteristic diameters of the particle size distribution, pycnometric density (ρ_p), fluidization classifications according to Geldart (Geldart, 1973), and minimum fluidization velocities (v_{mf}) calculated using Grace's correlations (Grace, 1986). These correlations, which compile extensive experimental data, provide valuable insights into fluidization behavior. Geldart's correlation, introduced approximately 50 years ago, describes fluidization behavior based on the density difference and particle size (using $d_{3,2}$ here). Grace's correlation further elucidates the fluidization regime by considering the superficial gas velocity, air in this case, and the mean particle diameter (d_{50}).

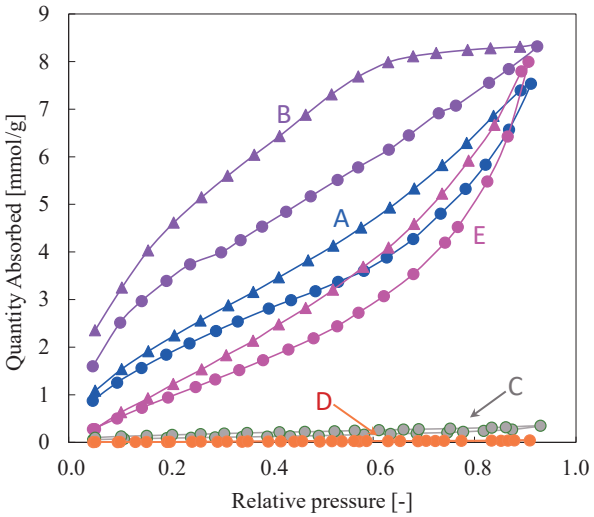

Fig. 2 Water sorption isotherms of powders at 25 °C: **A)** Avicel PH102, **B)** Wheat flour T45, **C)** Joint Filler, **D)** Glass beads (GB 3000E and GB-A), and **E)** RetaLac. Sorption curves are indicated by circular data points (○) and desorption curves by triangular data points (△).

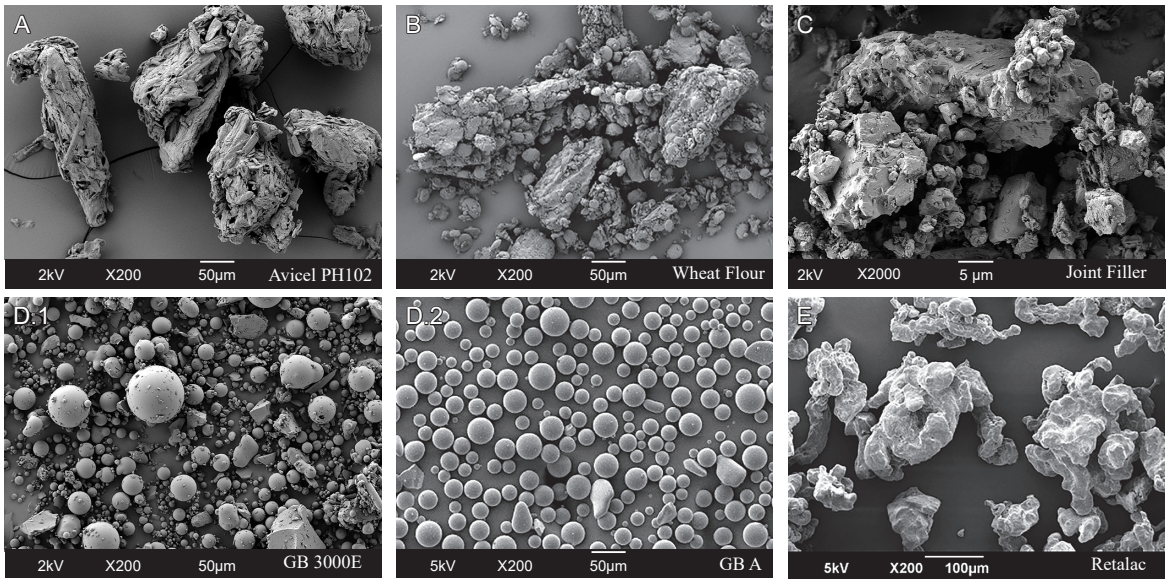

Fig. 3 Scanning electron microscopy (SEM) micrographs at different magnifications of the principal powders used in the study **A)** Avicel PH102, **B)** Wheat flour T45, **C)** Joint Filler, **D)** Glass beads, **D.1** GB 3000E and **D.2** GBA and **E)** RetaLac.

Table 1 Physical properties of samples.

Powder	Particle size distribution [μm]					ρ_p [a] [kg m^{-3}]	Geldart type	v_{mf} [10^{-3} m s^{-1}]
	d_{10}	d_{50}	d_{90}	$d_{4,3}$	$d_{3,2}$			
Avicel PH-102	35	111	225	122	69	1550	A	3.10
Wheat flour	17	83	177	91	25	1460	C-A	0.38
Joint filler	2	18	72	29	6	2810	C	0.04
GB 3000E	4	24	60	29	8	2660	A	0.07
GB-A	24	34	49	36	33	2490	A	1.14
RetaLac	47	191	415	222	132	1420	B	10.4

[a] Envelope density of the particles (equal to the pycnometric density for non-porous particles).

The particle size distribution was determined by laser diffraction (PSD-LD) in a liquid medium (ethanol) using a Mastersizer 3000 (Malvern Instruments). Morphological characterization was performed using scanning electron microscopy (SEM) with a Gemini 3 from Zeiss, equipped with a field-emission gun operating at 2 kV. The PSD-LD results indicate that RetaLac, Avicel PH102, and wheat flour consist of larger particles, while joint filler and glass beads exhibit a similar PSD with smaller particle sizes. The SEM micrographs in **Fig. 3** reveal the morphology of the samples. With the exception of GB-A, most samples display heterogeneity in size, shape, and surface roughness. Avicel PH102 particles have an isometric rod shape with a rough surface. RetaLac appears to be composed of agglomerates of amorphous-like particles. Wheat flour consists of irregularly shaped gluten and starch, with starch partially covering the gluten particles in a globule-like structure. The joint filler exhibits an uneven shape with flat surfaces, while GB-3000E is mostly spherical, though with some surface irregularities.

According to Geldart's classification, RetaLac is categorized as a Class B powder, characterized by smooth and homogeneous fluidization with minimal bubbling. Wheat flour falls between cohesive (Class C) and aeratable (Class A) powders. Joint filler is classified as a cohesive powder (Class C). Avicel PH102 and glass beads are both classified as Class A powders, which are associated with more pronounced bubbling during fluidization. Notably, GB 3000E exhibits greater cohesiveness compared to GB-A.

2.2 Experimental setup

To investigate the conditions that facilitate the compaction and decompaction of the powder bed, harmonic signals were generated with variations in amplitude and frequency. The experimental setup includes an electromagnetic shaker (BK vibration exciter 4809) connected to a cylindrical borosilicate glass vessel (26 mm in diameter and 240 mm in height), as shown in **Fig. 4**. The container weighs 72 g. The excitation system comprises a custom-made signal generator and a power amplifier (B&K 2718).

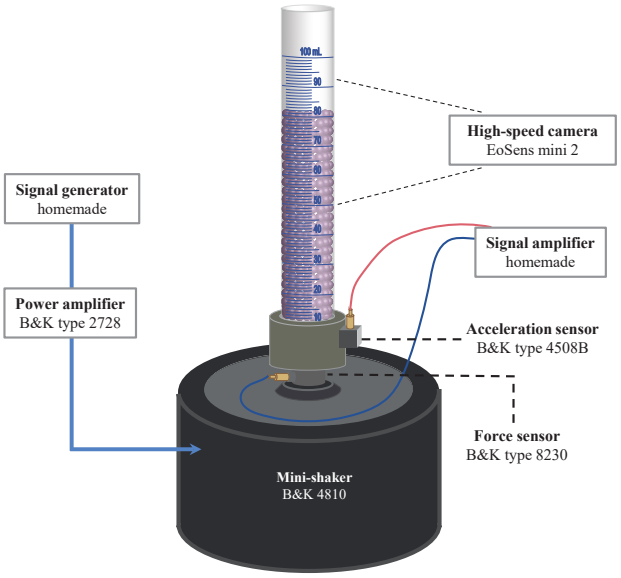

Fig. 4 Schematic representation of harmonically driven vibration experiments, including a particle damper, its excitation system, and data acquisition sensors.

Acceleration is measured using a DeltaTron® accelerometer (B&K 4508B) attached to the bottom of the vessel (**Fig. 4**). Force measurements are conducted using a force transducer (B&K 8230) mounted at the base of the container. Both excitation and data acquisition are controlled via LabVIEW. The height of the powder bed is captured via a high-speed camera (MotionBLITZ EoSens® mini 2), and the images are subsequently analyzed to determine the powder bed height, enabling the assessment of compactness dynamics and the Hausner ratio $HR(t)$ under various experimental conditions.

The compactness of the granular system can be quantified using various metrics, including the packing fraction ϕ, porosity $1-\phi$, and the void ratio $e = 1/\phi - 1$. While ϕ is more commonly used in granular physics (Suaza-Montalvo et al., 2023a), e is more commonly used in soil mechanics (Sonzogni et al., 2024). In dynamic systems, ϕ relates the volume of the particles V_p to the volume of the pile $V(t)$ at a given time, quantifying the available space for particle

reorganization within the bulk:

$$\phi(t) = \frac{V_p}{V(t)} = \frac{m_p}{V(t) \cdot \rho_p} \quad (1)$$

where ρ_p is the envelope density of the particles (equal to the pycnometric density for non-porous particles) and m_p is the powder mass.

HR, based on the pioneering work of Hausner (1967), is a measure commonly used in powder technology to assess flowability (Saker et al., 2019), though it mathematically reflects the compactness of the powder. It is defined as the ratio of the initial (loose) volume V_i to the tapped volume $V(t)$:

$$HR(t) = \frac{V_i}{V(t)} \quad (2)$$

Higher *HR* values indicate poorer flowability and greater cohesion among particles, which often correlates with increased compactness.

The densification dynamics are influenced by two primary factors: system geometry and vibration. System geometry encompasses variables such as grain size, vessel dimensions, and powder bed height. Vibration is governed by two dimensionless parameters: the relative acceleration, Γ, compares the imposed acceleration, a, to gravity, g:

$$\Gamma = \frac{a}{g} \quad (3)$$

and the relative frequency, Ω, compares the period, $2\pi/\omega$, to the time it takes for a grain to fall under gravity over a distance equal to its size, d:

$$\Omega = \frac{\omega}{\sqrt{g/d}} \quad (4)$$

The continuous densification methodology involves pouring the powder into a container using a funnel. Densification is then initiated by gradually increasing the acceleration of the imposed motion in steps at a fixed frequency. Each acceleration level is maintained until the powder bed stabilizes for at least 5 minutes. This stabilized state is considered quasi-static and is referred to as "stable compactness," denoted as $\phi_{s,i}(\Gamma_i)$. An entire experiment involves studying the relationship $\phi_{s,i} = f(\Gamma_i)$, until the powder bed undergoes decompaction. Since this is a continuous process, only the first acceleration step begins with the powder in an aerated state. Force and acceleration signals are depicted using peak-to-peak values of smoothed signals. The total error associated with each experimental data point was determined as described in previous works, accounting for both experimental and instrumental errors (Suaza-Montalvo et al., 2023a).

3. Results and discussions

The results section is structured as follows. We begin by demonstrating the high sensitivity of the force and acceleration signals to the dynamic behavior of the powders. Next, we delve into the densification dynamics. Finally, we aimed to characterize the force contact network at the mesoscale by drawing insights from the macroscopic results obtained through vibration-induced densification tests performed on different powders. It is important to note that our discussion of the results does not primarily focus on providing a detailed description or physical characterization of the powders used in this study. Instead, our powder selection effectively illustrates key phenomena and highlights significant findings. This approach was chosen to enhance the clarity and address the broad scope of the study.

In all figures where applicable, the results are presented in the following order: A: Avicel PH102, B: Wheat Flour, C: Joint Filler, D: Glass Beads (either 3000E or A type), and E: RetaLac.

3.1 Force and acceleration signals

In this study, dynamic densification experiments involving ϕ_s with Γ are conducted, during which all grains move in phase with the container, resembling macroscopically rigid inertial bodies. Nonetheless, a notable observation is that both force and acceleration signals are highly sensitive to particle movements. For example, during the initial seconds of excitation, depending on Γ, both force and acceleration signals can exhibit significant fluctuations (**Fig. 5A**), coinciding with the onset of fluidization phenomena (see Suaza-Montalvo et al., 2023b, Videos 06, 07, 08, and 09 in the DOREL repository for details). The fluidization of particles in these early moments of vibration can be attributed to the release of trapped air within the powder bed as it densifies (**Figs. 5B, C**). A key determinant of fluidization is the air velocity within the bed, v_{air}, which describes the rate of volume reduction over time:

$$v_{air} = \frac{1}{S}\frac{\Delta V}{\Delta t} \quad (5)$$

The determination and analysis of the average air velocity showed that when v_{air} surpasses the minimum fluidization velocity of particles, the bulk undergoes fluidization, as evidenced by the observations (**Fig. 5C**). As the v_{air} decreases, signaling reduced air availability, the densification of the bulk continues, resembling behavior more akin to solids on a macroscopic scale, and both the force and acceleration signals become stable. This phenomenon, consistent across various powders and vibration conditions, exemplifies the sensitivity of the force and acceleration signals in describing the dynamic response of the powder bed.

The differences in the signals can be attributed to the mass experienced by the system. As fluidization phenomena increase, the duration of particle flight between collisions with the container also increases. This trend continues

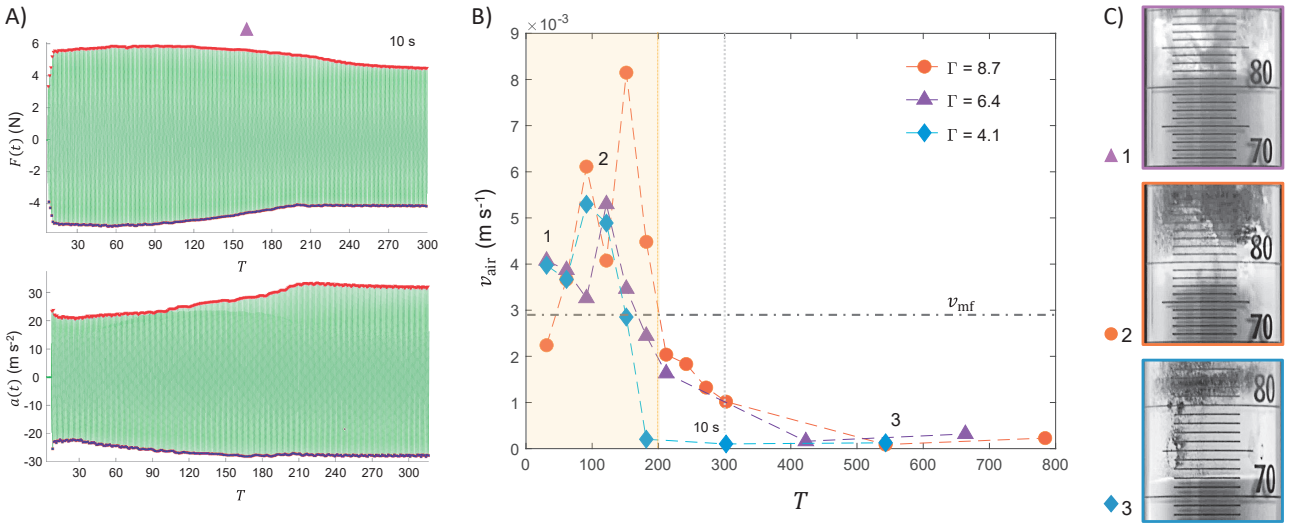

Fig. 5 **A)** Evolution of force and acceleration signals for Avicel PH 102 with the period T. **B)** Accompanied by an average estimation of air velocity evolution with T at various Γ values. **C)** Snapshots illustrating the observed behaviors of the powder bed.

until the air velocity decreases. Consequently, during fluidization, the average contribution of the grain mass felt by the container decreases. This mass is generally referred to as the dynamic mass of the granular sample, representing the portion of the grain mass that is effectively perceived by the container (Masmoudi et al., 2016; Meyer and Seifried, 2023).

The sensitivity of force and acceleration signals to packing density states and grain characteristics suggests that these signals can serve as structural descriptors, which may be more relevant to rheology than purely geometrical descriptors such as radial pair distributions.

3.2 Packing dynamics

Dynamic densification tests were conducted to investigate how vibration affects both force transmission and particle-scale interactions, focusing on macroscopic measurements. It is interesting to note that when decompaction conditions (Γ_d and F_d) are applied to an aerated powder, the powder may initially compact slightly, displaying either liquid-like, gas-like, or combined behaviors. It then reaches a convective state, after which it can decompact. This convective state can be sustained through several perturbations until suddenly the movement of the grains leads to the reintroduction of air into the bed, facilitating the decompaction process (see Suaza-Montalvo et al., 2023b, Video 16 in the DOREL repository for details).

The subsequent subsections present results from a series of experiments exploring the impact of frequency, sample conditioning (free-water), the shape of the force signal, and powder height.

3.2.1 The effect of relative frequency Ω on packing dynamics

The evolution of packing fraction ϕ_s with respect to Γ and Ω for Avicel PH102 and wheat flour is depicted in **Fig. 6**. The compaction dynamics vary depending on the powder type but follow a similar trend. At a constant Ω, an increase in Γ leads to an initial rise in the packing fraction until it reaches its maximum compaction state. Subsequently, further increases in vibration amplitude result in the decompaction of the powder bed, as illustrated by the star data points in **Fig. 6**. Decompaction may occur either gradually, with a convection-like motion inducing the aspiration of air into the powder bed, or abruptly, creating a powder cloud that impedes volume measurement. Specifically, lower frequency signals, as observed in samples such as RetaLac, wheat flour, and sericite, resulted in an explosive decompaction of the bed at lower acceleration levels compared to the 100 Hz driven signal.

Two general observations emerge from these experiments. Firstly, for low-cohesive samples such as GB A (**Fig. 6D**) and RetaLac (**Fig. 6E**), the densification dynamics are independent of the vibration frequency, as typically reported in the literature for glass bead-based studies (Ribière et al., 2007; Suaza-Montalvo et al., 2023a). Secondly, an increase in Ω induces powder bed decompaction at higher Γ values. Two possible explanations can be drawn from this last statement.

First, the kinetic vibration energy E_v for a harmonically driven system can be expressed as

$$E_v = \frac{m_p\, d\, g}{2}\left(\frac{\Gamma}{\Omega}\right)^2 \tag{6}$$

From this equation, it can be inferred that increasing Γ results in an increase in the kinetic vibration energy supplied to the powder bed. Conversely, increasing Ω reduces the kinetic vibration energy. Additionally, this phenomenon is closely related to energy dissipation. Notably, even under steady-state conditions, the dissipated energy can vary

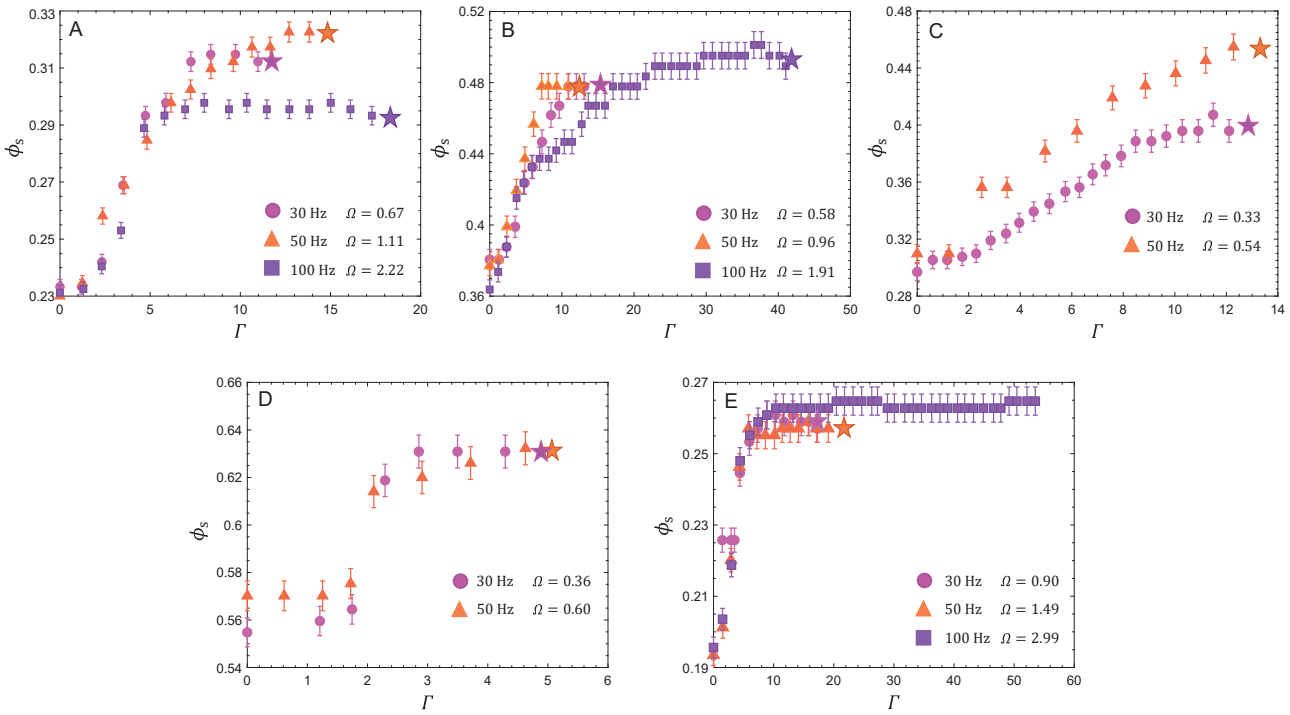

Fig. 6 The evolution of ϕ_s as a function of frequency and relative frequency Γ for **A)** Avicel PH102 at 20 % RH, **B)** Wheat Flour T45 at 60 % RH, **C)** Joint Filler at 60 % RH, **D)** GB-A at 20 % RH, and **E)** RetaLac at 20 % RH. The star denotes the relative frequency at which powder bed decompaction occurs.

from one period to another due to the complex nonlinearities in granular damping. This complexity is further amplified in cohesive powders, which exhibit cluster-like behaviors, making the analysis more demanding. Therefore, considering a more general expression to average behaviors can be prudent for analysis. Several expressions have been proposed to determine the maximum achievable energy dissipated in vibrated granular materials such as glass beads (Marhadi and Kinra, 2005; Masmoudi et al., 2016; Sack et al., 2013; Terzioglu et al., 2023), differing by scaling terms. In the solid-like state, observed just before decompaction, the particles do not lift off the container bottom (Suaza-Montalvo et al., 2023b, Video 04). Consequently, very little relative motion occurs between the particles. Recently, Meyer and Seifried (2023) described the energy dissipated per cycle during solid-like behavior, denoted as $\tilde{E}_{\text{diss}}$, as approximately 0.1 % of the particles' kinetic energy. The formula is given by

$$\tilde{E}_{\text{diss}} = \frac{\pi}{1000} m_{\text{p}} \left(\frac{\Gamma g}{\omega} \right)^2 \tag{7}$$

Eqn. (7) does not account for cohesion, which is typically observed in powders. However, calculating $\tilde{E}_{\text{diss}}$ at each decompaction point shows that higher dissipation energies are obtained for samples decompacting at larger Γ values. This indicates that as the vibrational amplitude increases, more energy is dissipated within the system, potentially influencing the overall behavior and stability of the powder bed.

3.2.2 The effect of conditioning (air-humidity) on packing dynamics

In this section, the influence of air humidity on ϕ_s concerning Γ was investigated by conditioning the samples at 20 % and 60 % RH. It's noteworthy that each powder possesses unique adsorption/absorption kinetics (**Fig. 2**) and reaches equilibrium at different rates. Consequently, after one week of conditioning, samples may exhibit varying water activities (a_w)—free or non-chemically bound water—despite following the same conditioning protocol. For instance, powders such as Avicel PH102 and RetaLac quickly reach equilibrium, with their a_w values aligning well with the relative humidity of the conditioning environment. However, other samples, such as Joint Filler, require longer conditioning periods.

The evolution of the packing fraction, ϕ_s, with respect to Γ and RH for all samples is shown in **Fig. 7**. The figure illustrates how conditioning at higher relative humidity can impact compaction dynamics, potentially increasing or decreasing the energy required to decompact the bed depending on the nature of the powder. Interestingly, the compaction dynamics appear to be independent of, or non-linearly related to, the powder's behavior towards water. For instance, low-adsorption samples such as GB 3000E (**Fig. 7D**) and Joint filler (**Fig. 7C**) show no statistical differences in compaction dynamics with increasing RH. A similar trend was observed for water-absorbing samples like wheat flour (**Fig. 7B**). Notably, air humidity does not affect the decompaction of GB 3000E.

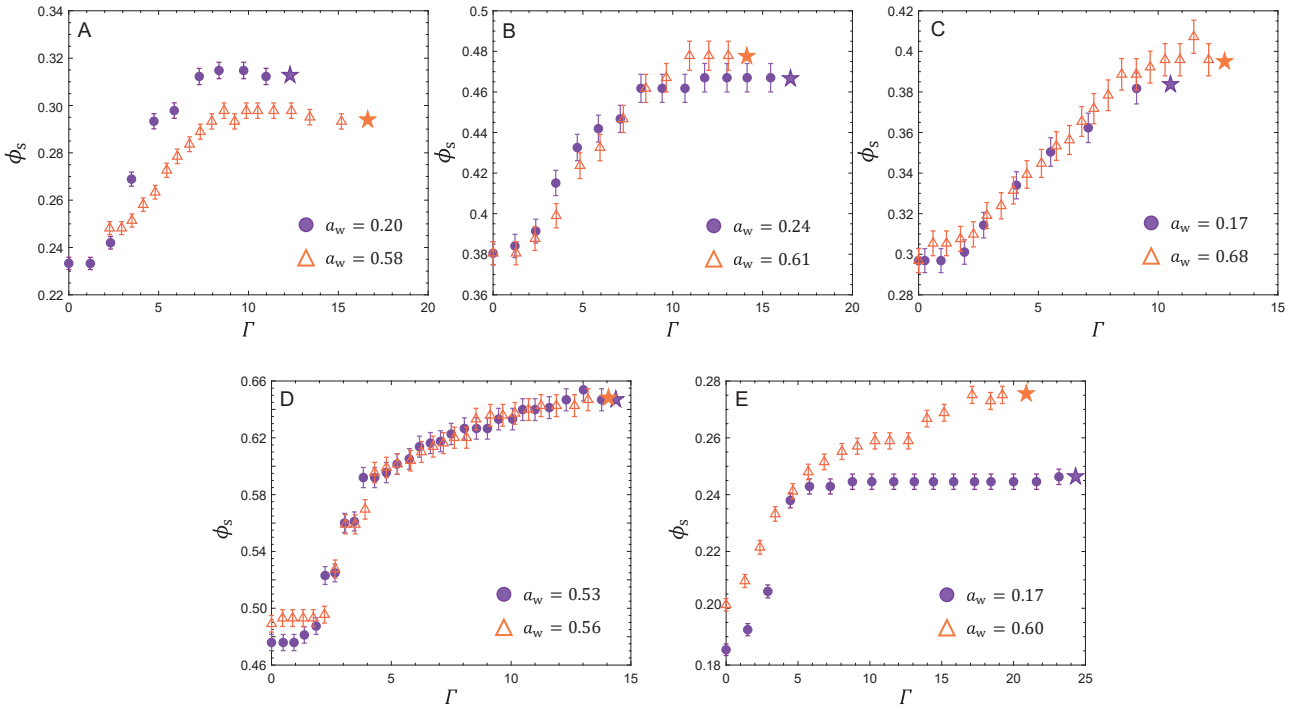

Fig. 7 The evolution of ϕ_s as a function of Γ at a fixed vibration frequency of 30 Hz for samples conditioned at different relative humidities (RH): ○ 20 % RH and △ 60 % RH, is shown for **A)** Avicel PH102, **B)** Wheat flour T45, **C)** Joint Filler, **D)** GB 3000E, and **E)** RetaLac. The star denotes the relative frequency Γ_d at which powder bed decompaction occurs.

The effect of RH on fine glass beads has been previously studied by Landi et al. (2011), who demonstrated that cohesion increases with air humidity. However, they concluded that only a small portion of the total condensed water on a single sphere forms capillary bridges. Furthermore, the strength of the interaction is weak because glass beads are chemically inert to water. This might explain why no changes in decompaction are observed for GB 3000E when exposed to different RH. Indeed, the a_w values obtained for glass beads are more reflective of environmental conditions. Therefore, GB 3000E exhibits statistically similar dynamics and serves as a good example of the excellent repeatability of the experiments.

For Avicel PH 102 and RetaLac, increased air humidity can either decrease or increase the packing fraction, respectively. Both powders are hydrophilic and absorb water at low moisture content (**Fig. 2**), with Avicel PH-102 being more hydrophilic and having smaller particles than RetaLac. These results highlight the challenges in drawing general conclusions based on physical properties such as particle size distribution, shape, and behavior towards water. A common trend observed among the samples is that, at a fixed frequency, lower packing fractions correspond to larger Γ_d (**Fig. 7**). This indicates that less compacted samples require more energy for decompaction. This phenomenon can be attributed to force transmission through the powder bed. Assuming that the contact network, or force network, formed by chain-like structures serves as preferential pathways for force transmission, it must be closely related to the geometric arrangement of the particles. The average number of contacts per particle, Z, is expected to be smaller for loosely packed fractions compared to more compacted ones. A smaller Z implies that fewer paths are available for force propagation, which ultimately influences the distribution of forces and promotes energy dissipation. Additionally, the strength of the contact can be influenced by the formation of liquid bridges.

In summary, individual particle properties alone cannot be linearly or easily related to packing dynamics, making straightforward conclusions challenging. However, the combination of these properties—such as size, shape, chemical nature of the surface, and condition—plays a significant role in mesoscale phenomena. From a mesoscale perspective, the overall behavior is influenced by the joint effects of multiple particle properties. For instance, size and shape affect the coordination number Z, which in turn influences packing dynamics. Therefore, the interplay between these properties at the mesoscale is crucial for understanding packing and compaction behavior. These experimental findings suggest that the dynamic parameters governing powder bed decompaction offer insights into mesoscale behavior, describing the contact force network from a macroscopic perspective.

3.2.3 The effect of force wave shape on packing dynamics

To better understand the influence of force wave shape on densification dynamics, damping experiments are

compared with uniaxial compaction experiments conducted under zero shear conditions. This experimental approach is based on the forces exerted on the system. Due to differences between devices, such as vessel geometry and powder content—fixed at 10 mL for FT4, while the powder mass is constant at 30 g for PD—the comparison is conducted using the specific energy E_m, determined from the force signal applied to the powder bed as follows:

$$E_m = \frac{F\Delta z}{m_p} \tag{8}$$

where Δz is the change in bed height.

For the compaction experiments with the FT4 compression cell, F is the force applied to the bed by the vented piston (**Fig. 1A**), as thoroughly described in a previous work (Cares-Pacheco et al., 2021). In summary, the piston compresses the sample in increments of force from 2 to 40 N at a rate of 0.4 N/s. For each increment, the piston maintains the force for 60 seconds to reach a steady state, after which the volume change with respect to the applied load is measured.

From **Fig. 8**, it can be observed that uniaxial compression and vibration-induced densification (step-like dynamics) methods exhibit similarities for cohesive powders. For easily flowing powders such as Avicel PH102 (**Fig. 8A**), particles tend to separate, move, and perform free parabolic flights during damping experiments, potentially leading to higher probabilities of reorganization. This capacity allows them to form denser organizational structures through vibration, as the restrictions imposed by the piston are reduced under similar energy provided to the system (see Suaza-Montalvo et al., 2023b, Videos 06 and 07 in the DOREL repository for details). Conversely, for more cohesive powders like wheat flour (**Fig. 8B**; see Suaza-Montalvo et al., 2023b, Video 08) and joint filler (**Fig. 8C**), particle separation into individual entities is more challenging. Compaction in these cases appears to occur through the movement of agglomerates, resulting in cluster-like behavior and reduced particle rearrangement. Zhao et al. (2021) explored the influence of vibration on wheat flour, highlighting that densification primarily involves smaller particles occupying interparticle voids, resulting in a denser bulk material with reduced permeability. Such behavior is also expected in uniaxial compression tests at low stress and may explain the similarities in the dynamics of densification observed between the two methods.

The significant difference between the FT4 and PD packing fractions for joint filler at 30 % RH may stem from its lower elastic modulus (**Table 2**), potentially influencing particle deformation.

3.2.4 The effect of volume fraction on packing dynamics

The effect of bed height on compactness is illustrated in **Fig. 9**. Experiments were carried out at three vessel filling fractions. The first filling fraction corresponded to a volume of 15 mL, resulting in a column height of 2.9 cm; the second to 50 mL, approximately half of the container, resulting in a height of 9.6 cm; and the third to the maximum filling of the measurable volume, which was 100 mL, resulting in a column height of 19.2 cm.

Several general observations arise from these experiments, as shown in **Fig. 9**. Firstly, ϕ_s increases with powder height, indicating that higher fillings lead to higher compactness. Secondly, low-volume fillings tend to have problems achieving high compaction levels. Notably, wheat flour shows intriguing behavior, as it does not exhibit clear densification at low or medium filling volumes (**Fig. 9B**). Similarly, glass beads 3000E do not densify at low volumes; instead, they maintain a convective, fluid-like behavior within the bulk while maintaining a relatively constant bulk height (**Fig. 9D**). This behavior is consistently observed with glass beads and can be visually observed at a macroscopic level, especially with larger particles, as depicted in **Fig. 10**, where some GB A particles were colored to follow their path.

As shown in **Eqn. (7)**, common trends closely relate the dissipated energy to the number of grains, as the loss factor monotonically increases with the mass of the powder (Masmoudi et al., 2016). This aligns with our findings, which demonstrate the challenges in compacting powder at low volumes.

The relationship between the force required to decompact the powder bed and the powder volume is surprisingly non-monotonic (**Fig. 9**). Medium-volume powder columns consistently decompact at lower Γ values, indicating that the force does not follow a simple, consistent trend with increasing or decreasing volume. Instead, the required force exhibits complex and fluctuating behavior as the volume changes, suggesting that other factors or interactions are influencing the decompaction force in a non-linear manner. While dissipation initially appears to be a major contributing factor, it does not fully explain why medium volumes decompact at lower accelerations.

When the powder bed is mechanically excited, compression waves or shear waves propagate from the point of excitation. As the grains interact with this external field through scattering and absorption, the field can also exert forces on them. This elastic longitudinal wave moves through the material at a velocity, c, that can be determined as

$$c = \sqrt{\frac{E_{el}(1-\nu)}{\rho(1-2\nu)(1+\nu)}} \tag{9}$$

where E_{el} is the Young's modulus, ν is the Poisson's ratio and ρ the density of the material, here represented by the pycnometric density, ρ_p.

The elastic modulus of the powders has been determined

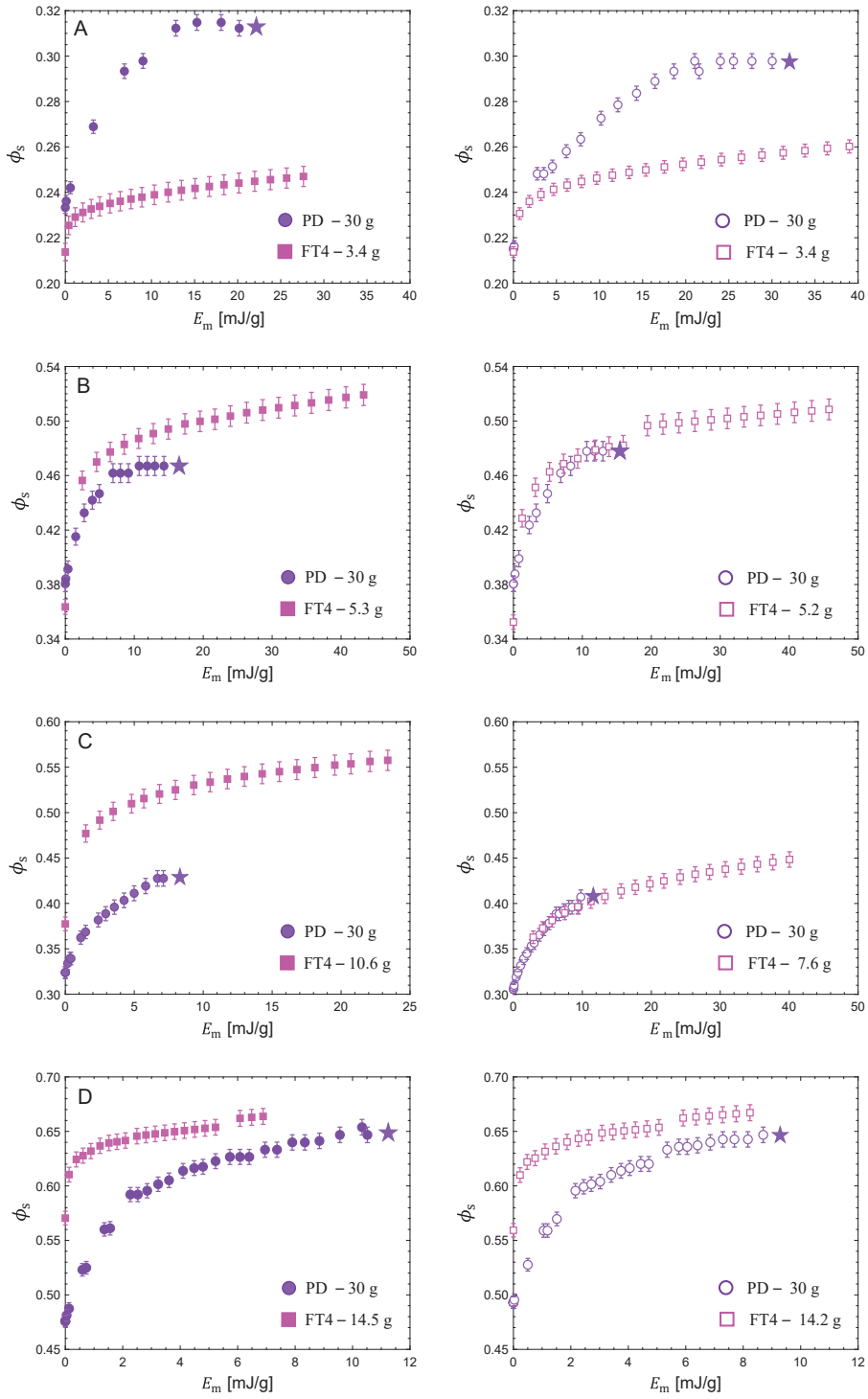

Fig. 8 Dynamic densification ϕ_s as a function of E_m. Compaction is generated using a particle damper (PD) at f = 30 Hz (○) and uniaxial compression with the FT4 (□). Filled symbols represent samples conditioned at 20 % RH **(left)**, and empty symbols represent samples conditioned at 60 % RH **(right)**. The star indicates the E_m at which powder bed decompaction occurs. The data are shown for **A)** Avicel PH 102, **B)** Wheat flour, **C)** Joint filler, and **D)** GB 3000E.

in previous works using the apparent mass vibration method, as described in Cares-Pacheco et al. (2024). This methodology evaluates the elastic properties of the powders under aerated conditions, and under these conditions, v is neglected. As a result, the velocity c of the elastic longitudinal wave is simplified to $c = \sqrt{E_{el} / \rho_p}$. The wavelength λ of the wave propagating through the powder can be determined using the relationship $\lambda = c/f$, where f is the driven frequency.

The results are presented in **Table 2**. It is important to note that **Eqn. (9)** assumes the material is isotropic and homogeneous, meaning its properties are consistent in all

directions. This assumption may not hold true for all materials, and deviations from isotropy or homogeneity could affect the accuracy of the calculated wave velocity and wavelength. However, this approach still provides a reasonable approximation for the interpretation of the experimental data.

Table 2 Calculations of the velocity c, and wavelength λ, of the vibration propagating within the powder bed, determined from the powder's elastic modulus E_{el}[b].

Powder	E_{el} [MPa]	c [m/s]	λ [m]
Av. PH102	0.20	12.5	0.32
GB-3000E	0.57	13.8	0.65
Wheat flour	0.24	15.4	0.46
Joint filler	0.17	20.7	0.27

[b] Cares-Pacheco et al. (2024)

Since only the first mode of propagation is expected within the vessel (Gaete-Garretón et al., 2007), the theoretical longitudinal wave transmitted to the powder, as described in **Table 2**, is depicted in **Fig. 11**, along with the filling volumes used during the experiments. It is observed that higher compression—wave crest—is expected for medium and maximum fillings. However, dissipation increases with the number of particles (Marhadi and Kinra, 2005). Therefore, particles at medium fillings, experiencing higher compression but lower dissipation, might

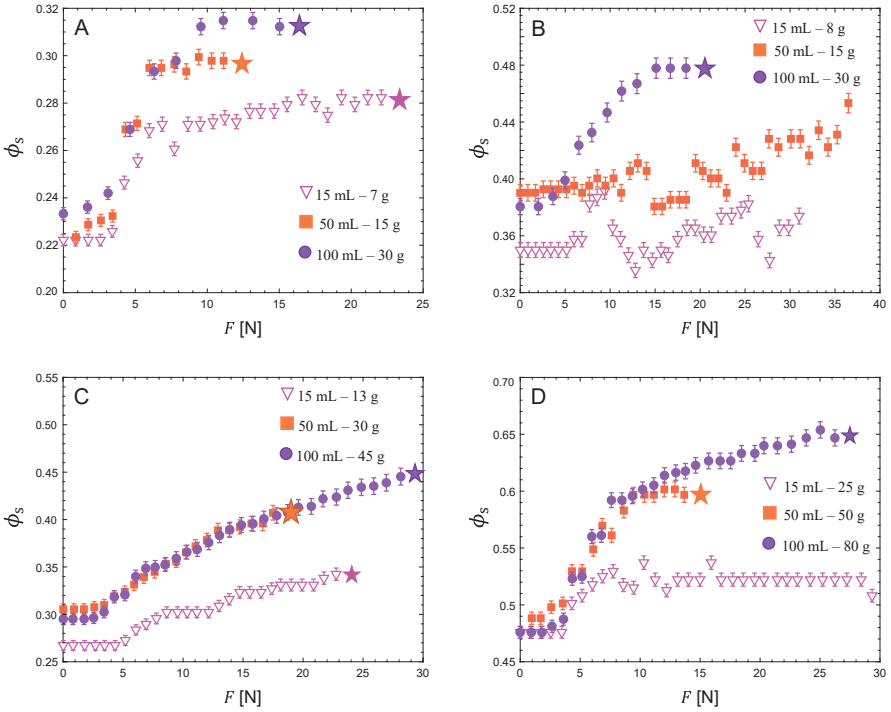

Fig. 9 The densification dynamics of ϕ_s as a function of F, where ϕ_s is investigated at a fixed f = 30 Hz for different volumes: low volume, ▽ 15 mL; medium volume, □ 50 mL; and full volume, ○ 100 mL. Samples include **A)** Avicel PH102 conditioned at 30 % RH, **B)** wheat flour conditioned at 30 % RH, **C)** joint filler conditioned at 60 % RH, and **D)** GB 3000E conditioned at 30 % RH. The star indicates the force at which powder bed decompaction occurs.

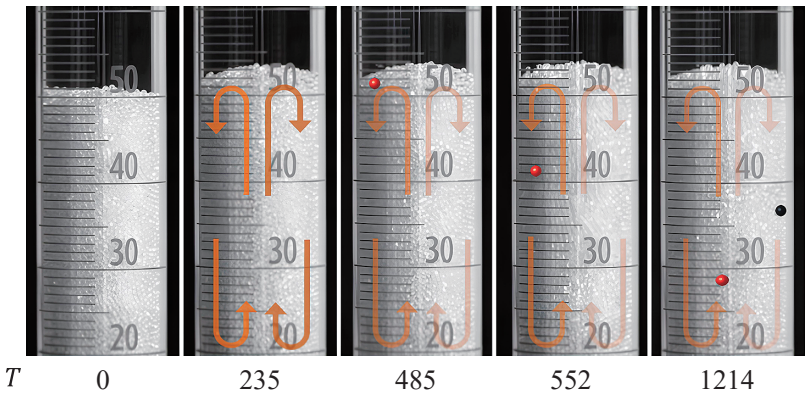

Fig. 10 Convective movement observed with GB-A. Some particles were colored red and black to track their path.

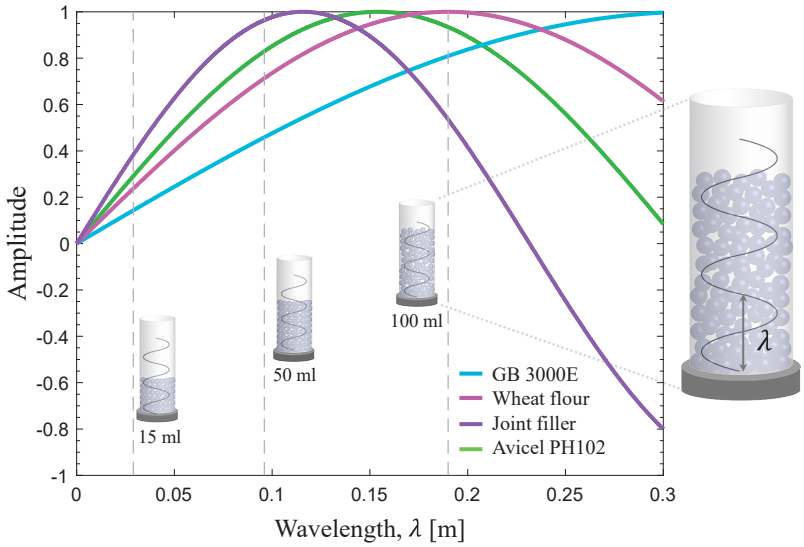

Fig. 11 Theoretical longitudinal wave (LW) propagating within the powder column from **Table 2**, with vertical dashed lines delineating the powder volume in the vessel. The diagram shows the direction of LW propagation through the powder.

decompact more easily at lower accelerations.

This simplified analysis of the transmission of vibration waves from the experiments (**Fig. 11**) shows potential. Indeed, the length and shape of the vibration propagating within the material can be correlated with the acoustic impedance of the system (transducer + container + media) (Hueter and Bolt, 1955). It has been demonstrated that the acoustic impedance response of the system varies with column height, leading to completely different dynamic behaviors. For instance, for wood particles immersed in water, at low acoustic impedance, the particles exhibited agglomeration with a large cluster-like structure at the center of the suspension, while a highly dispersive granular suspension was observed at the maximum impedance regime (Cares-Pacheco et al., 2010; Gaete-Garretón et al., 2011).

Recently, Sonzogni et al. (2024), using particle dynamic simulations, concluded that the void ratio e, in isotropic compaction depends in a nonlinear and nonmonotonic way on the degree of adhesion of monodisperse hard particles. Our experiments appear to validate this statement; however, it is important to note that the degree of cohesion in real samples cannot be isolated from other particle properties, such as elastic modulus, size, and shape. The combined effects of these factors may also contribute to the observed behaviors, making it challenging to attribute the dynamics solely to cohesion.

3.3 Decoding attractive interactions

Despite conditioning the powder and implementing strict pouring protocols to achieve a highly reproducible initial packing fraction and constant powder height, the authors acknowledge the extremely low probability of reproducing the same contact network after pouring the

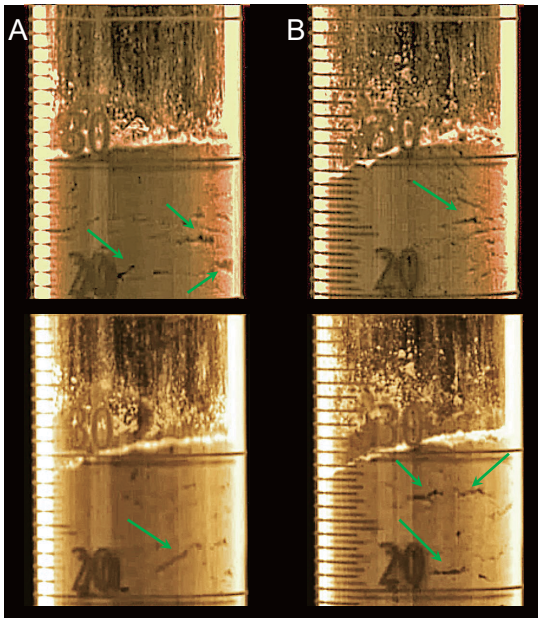

Fig. 12 Snapshots from two separate compaction dynamics experiments, **A** and **B**, on different samples of the same powder under identical vibration conditions. The images, captured at synchronized intervals, compare the dynamics at two different moments (**top** and **bottom** sets). Green arrows highlight differences in particle rearrangement within the bulk.

powder. For instance, **Fig. 12** shows two distinct experiments for the same sample under identical excitation conditions (see Suaza-Montalvo et al., 2023b, Video 03 in the DOREL repository for details). Although both samples achieved a reproducible packing evolution $\phi(t)$, with less than 2 % variability, image analysis revealed that particles within the bulk follow different trends, indicating that the contact network itself, and its evolution during vibration are not identical but statistically retain a consistent packing

fraction. This underscores the challenges in describing force contact networks in 3D configurations and highlights the difficulties, or even the irrationality, of comparing experiments with theoretical modeling at the grain scale for such configurations. The particles can assume virtually infinite packing configurations while statistically retaining consistent macroscopic properties.

The anisotropy in the contact network prompts us to focus on identifying indicators that offer meaningful insights into the system dynamics. In this regard, the decompaction conditions (Γ_d and F_d) are applied to the granular material, irrespective of its packing state, the powder bed will not be able to compact. Instead, a fluid-like behavior, either liquid-like or gas-like, or both, will be observed, indicating an unstable state. Such experimental findings allow us to infer that the parameters facilitating the decompaction of a powder bulk provide insights into the mesoscale, macroscopically describing a limit of stability in the contact network. In this context, Γ_d serves as a descriptor of bulk cohesion. A dimensionless number can be defined from it as the ratio of cohesive forces to non-cohesive forces:

$$A_d = \frac{F_d}{W_p} \tag{10}$$

Eqn. (10) is akin to a Bond number of the mesoscale, quantifying bulk adhesion as the ratio of decompaction force to the gravitational weight of the powder, W_p. A strong force network is characterized by $A_d > 1$, while $A_d < 1$ values will denote a weak contact network.

The decompaction force relies on both the vibration wave (its shape and intensity—Ω, Γ, but also the period between cycles) and the system geometry (container dimensions, grain size, and powder height). This implies that various configurations can be explored, each corresponding to specific conditions under study. Nevertheless, the *maximum packing fraction* ϕ_U, can be identified for a fixed system geometry, representing the highest achievable reorganization state of the powder in a vessel. This fraction is intrinsic to the powder and appears to correlate more closely with the powder's flowability assessment when using the *HR* (Saker et al., 2019). This maximum consolidation state is referred to as the "Ultimate" state, and all parameters describing it are denoted by the subscript *U* (e.g., $F_{d,U}$ and HR_U). This ultimate consolidation state ϕ_U, can be determined either through continuous experiments, like those conducted in this study, or through stationary studies, as elaborated in Suaza-Montalvo et al. (2023a).

The relationship between the ultimate Hausner ratio HR_U as a flow indicator and cohesive interactions from $F_{d,U}$ values, for our fixed geometry and various powders (30 g of powder and 20 % RH) is depicted in **Fig. 13**. Here, the HR_U values show a linear increase with A_d (plotted on a semi-logarithmic scale). This observation supports our hypothesis, indicating that lower A_d values are associated with a weak force network, where W_p outweighs cohesive interactions, as typically seen in gravitational flows. Conversely, higher A_d values are linked with strong networks that hinder flow.

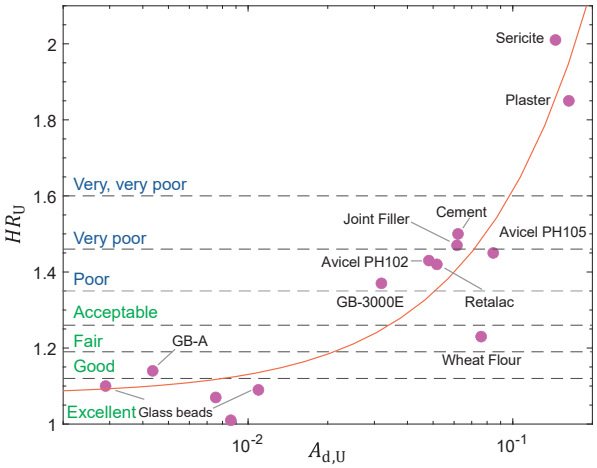

Fig. 13 Evolution of HR_U with $A_{d,U}$, both determined from the experiments where the highest packing fraction was obtained. The *y*-axis shows the Hausner classification of flowability.

It can be observed that wheat flour deviates from the expected trend, and Avicel PH102 is described as having poor flowability. For wheat flour, which consists mainly of gluten and starch, fair flowability can be attributed to its bi-modal particle size distribution and elastic properties, with gluten particles being larger and harder than starch particles (Cares-Pacheco et al., 2024). In the case of Avicel PH102, a powder formulated for compaction, its aptitude for compaction does not directly correlate with its ability to flow. However, this may explain the presence of a medium-strength force network; despite the low cohesion between particles (with a Bond number of 14), particle deformation during compaction increases the number of contact points.

In an effort to delve deeper into our potential contact network descriptor $A_{d,U}$, **Table 3** compiles dimensionless cohesion descriptors derived from previous studies. These descriptors were obtained using techniques such as Inverse Gas Chromatography (IGC) (Jiménez-Garavito et al., 2023) and shear test experiments (Cares-Pacheco and Falk, 2023). Notably, the dispersive surface energy γ_s^d is highlighted as a powerful descriptor of the surface properties of divided solids, indicating cohesion at the particle scale. This is represented by the granular Bond number Bo_g, which relates interparticle cohesion F_c to the particle weight W_g as follows, based on the multi-asperity model by Chen et al. (2008):

$$F_c = \frac{H}{12 z_0^2}\left(\frac{d}{2(L_0 / z_0)^2} + \frac{3 d_a d}{d_a + d}\right) \tag{11}$$

where L_0 is the separation distance, set at 0.1 μm; d_a is the

Table 3 Summary of attractive interparticle forces descriptors at different scales, with the dispersive surface energy (γ_s^d) used to determine the granular Bond number (Bo_g[c]) as a particle-scale descriptor, the parameter C[d] from shear testing as a bulk-scale descriptor, the flow factor (f_c), and $A_{d,U}$ as a mesoscale descriptor of the contact network, with the ultimate Hausner ratio (HR_U) serving as its flow index.

Powder	IGC[c]		FT4[d]		PD decompaction	
	γ_s^d	Bo_g	C	f_c	$A_{d,U}$	HR_U
Avicel PH-102	57.8	14	0.027	17	48	1.43
Wheat flour	42.8	109	0.073	7	76	1.23
Joint filler	39.9	5681	0.064	7	62	1.47
GB-3000E	47.2	170	0.021	22	32	1.37

[c] Jiménez et al., 2023; [d] Cares-Pacheco and Falk, 2023.

asperities diameter, set at 0.2 μm; z_0 is the equilibrium separation distance equal to 0.4 nm; and H is the Hamaker constant, determined using Frenkel's relation:

$$H = 24\pi D_0^2 \gamma_s^d \tag{12}$$

with D_0 being the cut-off distance, equal to 0.165 nm.

The parameter C, which compares the adhesive interactions between grains as determined from the yield locus and the confining normal stress or preconsolidation stress in shear testing, serves as a critical bulk-scale descriptor (Cares-Pacheco and Falk, 2023). To ensure a comprehensive comparison under consistent consolidation conditions, the C and f_c values listed in **Table 3** were obtained at the same preconsolidation force at which powder decompaction occurs in our damping tests. This consistency ensures that the comparison across different descriptors is meaningful and reliable, particularly when assessing the mesoscale descriptor $A_{d,U}$ and the HR_U as a flow index.

The comparative analysis of the samples reveals distinct characteristics in their cohesion properties and contact networks. For Avicel PH-102, the moderate $A_{d,U}$ value indicates a well-established contact network. The relatively low C and Bo_g values suggest moderate bulk cohesion and interparticle forces, respectively. Wheat flour, on the other hand, exhibits higher Bo_g and C values, indicating strong interparticle forces and bulk cohesion. The high $A_{d,U}$ value indicates a robust contact network, likely contributing to the overall cohesion.

Joint filler displays an extremely high Bo_g signifying very strong interparticle cohesion, consistent with its high C. The high $A_{d,U}$ value further indicates a well-developed contact network, supporting the strong bulk properties. In contrast, GB-3000E had the lowest $A_{d,U}$, suggesting a less developed contact network compared to the other samples. The low C and moderate Bo_g values indicate weaker cohesion at both the particle and bulk scales. It's important to note that the analysis seems biased by the Bo_g values, particularly for GB-3000E and Joint filler. In these cases, the higher Bo_g values are more influenced by particle size distribution rather than accurately reflecting cohesive behavior, as observed with GB-3000E. This indicates that Bo_g may not always be a reliable indicator of cohesion, particularly when particle size distribution significantly affects the results.

From a broader perspective, a higher Bo_g generally corresponds to a higher C, indicating that stronger interparticle forces contribute to greater bulk cohesion. However, despite extensive research (Capece et al., 2015; Cares-Pacheco and Falk, 2023; Giraud et al., 2020), establishing a direct correlation between particle-scale properties and bulk properties from shear testing has been challenging, primarily due to the extreme sensitivity of Bo_g to particle size. Nevertheless, while bulk cohesion from the yield locus in shear testing is often categorized as a bulk property, it actually represents a fracture plane, providing a two-dimensional view of plastic failure phenomena. As a result, this parameter may not fully capture the essence of bulk cohesion, which is inherently a three-dimensional characteristic. The challenge lies in accurately linking these scales without relying solely on one specific physical property of the grains.

There is a notable correlation between C and $A_{d,U}$; a more robust contact network, indicated by higher $A_{d,U}$ often supports higher bulk cohesion, indicated by higher C. The $A_{d,U}$ parameter provides insight into the limitations of the contact network, offering a view into the mesoscale and reflecting how particles rearrange and interact beyond simple pairwise contacts. The discovery of a macroscale descriptor for the contact force network, which can be determined independently of particle size or any specific particle properties, holds significant promise for better modeling and understanding granular materials on a broader scale.

4. Conclusions

This study delved into the intricate dynamics of vibration-induced densification across a broad spectrum of industrial powders, including wheat flour, joint filler, glass beads, and pharmaceutical excipients. By utilizing a particle damper, we conducted an extensive series of

experiments to investigate the effects of frequency, air humidity conditioning, and powder height on densification dynamics. We consistently analyzed the evolution of packing fraction with acceleration to explore the conditions leading to compaction and decompaction.

Our findings illuminate the pivotal role of transmitted vibration waves in shaping the densification dynamics of granular materials, underscoring the significance of particle dampers. Notably, the sensitivity of force and acceleration signals to changes in packing density highlights their potential as structural descriptors of bulk material.

The results demonstrate that under decompaction conditions, the granular assembly does not reach a steady state but instead exhibits liquid-like, gas-like, or combined behaviors. The decompaction force appears to counteract interparticle forces, preventing particle cohesion. These experimental findings suggest that the dynamic parameters controlling the decompaction of the powder bed provide insights into the mesoscale, revealing limitations within the contact force network.

The comparison between adhesive interaction descriptors such as Bo_g and bulk cohesion C highlights that the $A_{d,U}$ parameter shows a notable correlation with C and can be similar to Bo_g. This indicates that a more robust contact network, as reflected in higher $A_{d,U}$ values, often corresponds to greater bulk and interparticle cohesion. The bulk cohesion parameter C, typically derived from the yield locus in shear testing, primarily represents a fracture plane, offering only a two-dimensional perspective on plastic failure and may not fully capture the three-dimensional nature of bulk cohesion. Unlike Bo_g, which is sensitive to particle size and reflects particle-scale properties, $A_{d,U}$ provides valuable insights into the mesoscale structure of the contact network, highlighting complex interactions beyond simple pairwise contacts. The potential of this macroscale descriptor for the contact force network, independent of particle size and specific particle properties, could significantly enhance the modeling and understanding of granular materials on a broader scale.

The results also highlight the importance of accurately quantifying the effects of air humidity on the samples. The water activity of the samples, representing free water, emerges as a suitable indicator that should be considered to ensure reproducible results and to better understand its role in particle interactions.

Consistent results, depending on particle nature and conditioning, highlight that simple, hard, cohesionless, round grains cannot adequately represent the intricate interactions between grains in real granular assemblies, which are often cohesive and possess arbitrary shapes. By extracting and comprehending realistic particle-scale and bulk-scale data, this research establishes a foundation for developing comprehensive, physics-based insights for effectively understanding the behavior of granular materials.

Future research should prioritize longitudinal wave propagation, acoustic impedance, and powder column height by using the experimental framework established here. Moreover, integrating theoretical data-driven models can complement experimental findings, providing a more nuanced understanding of the microscopic forces. This integration has the potential to enhance the predictive capabilities of existing models and provide valuable insights into the behavior of granular materials under diverse conditions.

Acknowledgments

The authors acknowledge Andrea Suaza-Montalvo, Maria Camila Jiménez-Garavito, and Assia Saker for their valuable contributions to the experimental work. The combined data laid the groundwork for this study.

Data Availability Statement

Some data supporting the findings of this study are openly available in the DOREL repository at the Université de Lorraine. The data can be accessed through the https://doi.org/10.12763/VKDBAS.

Nomenclature

a	acceleration (m s^{-2})
a_w	water activity (-)
A_d	ratio of cohesive to noncohesive forces (-)
$A_{d,U}$	ultimate A_d (-)
Bo_g	granular Bond number (-)
c	wave velocity (m s^{-1})
C	ratio of bulk cohesion to preconsolidation stress from shear testing experiments (-)
d_a	asperity diameter (m)
D_0	cut-off distance (m)
d	particle diameter (μm)
$d_{3,2}$	Sauter diameter (μm)
$d_{4,3}$	De Brouckere mean diameter (μm)
d_{10}, d_{50}, d_{90}	particles diameters corresponding to the 10th, 50th, and 90th percentiles (μm)
E_{el}	elastic (Young's) modulus (MPa)
E_m	specific energy (J kg^{-1})
E_v	kinetic vibration energy derived from harmonically driven systems (J)
$\tilde{E}_{diss}$	dissipated energy (J)
f	frequency (Hz)
f_c	flow factor derived from the shear test
F	force (N)
F_c	cohesion force derived from the multi-asperity model (N)
F_d	force at decompaction point (N)
$F_{d,U}$	ultimate force at decompaction point (N)
g	gravity (m s^{-2})
H	Hamaker constant (J)
HR	Hausner ratio (-)
HR_U	ultimate Hausner ratio (-)
L_0	separation distance (m)
m	mass (kg)
m_p	mass of powder (kg)
S	cross section of the vessel (m^2)

V	volume of a vessel (L)
W_p	powder weight (N)
W_g	particle weight (N)
v	velocity (m s^{-1})
v_{air}	average air velocity (m s^{-1})
v_{mf}	minimum fluidization velocity (m s^{-1})
Z	average number of contacts per particle (-)
z_0	equilibrium separation distance (m)
γ_s^d	dispersive surface energy (J m^{-2})
Γ	relative acceleration (-)
Γ_d	relative acceleration at decompaction point (-)
Δt	time duration (s)
ΔV	bed volume reduction (m^3)
Δz	bed height reduction (m)
λ	wavelength (m)
μ	gas viscosity (Pa s)
ν	Poisson's ratio (-)
ρ	density (kg m^{-3})
ρ_p	pycnometric density (kg m^{-3})
ϕ	packing fraction (-)
ϕ_s	stable packing fraction (-)
ϕ_U	ultimate packing fraction (-)
$\phi_{s,d}$	packing fraction at decompaction point (-)
ω	angular frequency (rad s^{-1})
Ω	relative frequency (-)

References

Andreotti B., Forterre Y., Pouliquen O., Les Milieux Granulaires—Entre Fluide et Solide, EDP Sciences, 2011. ISBN: 978-2759800971.

Bérut A., Pouliquen O., Forterre Y., Brownian granular flows down heaps, Physical Review Letters, 123 (2019) 248005. https://doi.org/10.1103/PhysRevLett.123.248005

Capece M., Ho R., Strong J., Gao P., Prediction of powder flow performance using a multi-component granular Bond number, Powder Technology, 286 (2015) 561–571. https://doi.org/10.1016/j.powtec.2015.08.031

Cares-Pacheco M.-G., Cordeiro E., Gérardin F., Falk V., Consistency in Young's modulus of powders: a review with experiments, Powders, 3(2) (2024) 280–304. https://doi.org/10.3390/powders3020017

Cares-Pacheco M.G., Falk V., A phenomenological law for complex granular materials from Mohr-Coulomb theory, Advanced Powder Technology, 34 (2023) 103888. https://doi.org/10.1016/j.apt.2022.103888

Cares-Pacheco M.-G., Jiménez Garavito M.-C., Ober A., Gerardin F., Silvente E., Falk V., Effects of humidity and glidants on the flowability of pharmaceutical excipients. An experimental energetical approach during granular compaction, International Journal of Pharmaceutics, 604 (2021) 120747. https://doi.org/10.1016/j.ijpharm.2021.120747

Cares-Pacheco M.G., Vargas Y., Gaete L., Sainz J., Alarcón J., Ultrasonically assisted extraction of bioactive principles from Quillaja Saponaria Molina, Physics Procedia, 3 (2010) 169–178. https://doi.org/10.1016/j.phpro.2010.01.024

Carson J.W., Wellwood G., Maynard E.P., How to reduce safety risks when storing and handling bulk solids, Informa Markets, (2019). <https://www.powderbulksolids.com/> accessed 16.05.2024.

Chen Y., Yang J., Dave R., Pfeffer R., Fluidization of coated group C powders, AIChE Journal, 54 (2008) 104–121. https://doi.org/10.1002/aic.11368

Gaete-Garretón L., Hernández Y., Cares M., Vega R., Influence of acoustic parameters in ultrasonic comminution of Zn powders in liquid phase, presented at the Internation Congress on Acoustics, ICA 19th, Madrid, 2007.

Gaete-Garretón L., Vargas-Hernández Y., Cares-Pacheco M.G., Sainz J., Alarcón J., Ultrasonically enhanced extraction of bioactive principles from Quillaja Saponaria Molina, Ultrasonics, 51 (2011) 581–585. https://doi.org/10.1016/j.ultras.2010.12.012

Geldart D., Types of gas fluidization, Powder Technology, 7 (1973) 285–292. https://doi.org/10.1016/0032-5910(73)80037-3

Ghadiri M., Pasha Mehrdad, Nan W., Hare C., Vivacqua V., Zafar U., Nezamabadi S., Lopez A., Pasha Massih, Nadimi S., Cohesive powder flow: trends and challenges in characterisation and analysis, KONA Powder and Particle Journal, 37 (2020) 3–18. https://doi.org/10.14356/kona.2020018

Gilabert F.A., Roux J.-N., Castellanos A., Computer simulation of model cohesive powders: influence of assembling procedure and contact laws on low consolidation states, Physical Review E, 75 (2007) 011303. https://doi.org/10.1103/PhysRevE.75.011303

Giraud M., Gatumel S., Vaudez S., Bernard-Granger G., Nos J., Gervais T., Berthiaux H., Investigation of a granular Bond number based rheological model for polydispersed particulate systems, Chemical Engineering Science, 228 (2020) 115971. https://doi.org/10.1016/j.ces.2020.115971

Grace J.R., Contacting modes and behaviour classification of gas—solid and other two-phase suspensions, The Canadian Journal of Chemical Engineering, 64 (1986) 353–363. https://doi.org/10.1002/cjce.5450640301

Hausner H., Friction conditions in a mass of metal powder, International Journal of Powder Metal, 3 (1967) 7–13.

Herrmann H.J., Hovi J.-P., Luding S., Eds., Physics of Dry Granular Media, Springer Netherlands, Dordrecht, 1998, ISBN: 978-0792351023. https://doi.org/10.1007/978-94-017-2653-5

Hueter T.F., Bolt R.H., Sonics: Techniques for the Use of Sound and Ultrasound in Engineering and Science, Wiley, 1955, ISBN: 9780471419761.

Jaeger H.M., Nagel S.R., Behringer R.P., Granular solids, liquids, and gases, Reviews of Modern Physics, 68 (1996) 1259–1273. https://doi.org/10.1103/RevModPhys.68.1259

Jiménez Garavito M.C., Cares Pacheco M.G., Witschger O., Bau S., Gerardin F., Falk V., The effect of silica nanoparticles on the dustiness of industrial powders, Advanced Powder Technology, 34 (2023) 104105. https://doi.org/10.1016/j.apt.2023.104105

Knight J.B., Fandrich C.G., Lau C.N., Jaeger H.M., Nagel S.R., Density relaxation in a vibrated granular material, Physical Review E, 51 (1995) 3957–3963. https://doi.org/10.1103/PhysRevE.51.3957

Kollmer J.E., Daniels K.E., Betweenness centrality as predictor for forces in granular packings, Soft Matter, 15 (2019) 1793–1798. https://doi.org/10.1039/C8SM01372A

Landi G., Barletta D., Poletto M., Modelling and experiments on the effect of air humidity on the flow properties of glass powders, Powder Technology, 207 (2011) 437–443. https://doi.org/10.1016/j.powtec.2010.11.033

Majmudar T.S., Behringer R.P., Contact force measurements and stress-induced anisotropy in granular materials, Nature, 435 (2005) 1079–1082. https://doi.org/10.1038/nature03805

Marhadi K.S., Kinra V.K., Particle impact damping: effect of mass ratio, material, and shape, Journal of Sound and Vibration, 283 (2005) 433–448. https://doi.org/10.1016/j.jsv.2004.04.013

Marteau E., Andrade J.E., An experimental study of the effect of particle shape on force transmission and mobilized strength of granular materials, Journal of Applied Mechanics, 88 (2021) 111009. https://doi.org/10.1115/1.4051818

Masmoudi M., Job S., Abbes M.S., Tawfiq I., Haddar M., Experimental and numerical investigations of dissipation mechanisms in particle dampers, Granular Matter, 18 (2016) 71. https://doi.org/10.1007/s10035-016-0667-4

Meyer N., Seifried R., Systematic design of particle dampers for transient vertical vibrations, Granular Matter, 25 (2023) 3. https://doi.org/10.1007/s10035-022-01290-y

Papadopoulos L., Porter M.A., Daniels K.E., Bassett D.S., Network analysis of particles and grains, Journal of Complex Networks, 6 (2018) 485–565. https://doi.org/10.1093/comnet/cny005

Radjai F., Topin V., Richefeu V., Voivret C., Delenne J.-Y., Azéma E., El Youssoufi M.S., Force transmission in cohesive granular media, in: J. D. Goddard J.T.J. et P.G. (Ed.), Mathematical Modeling and Physical Instances of Granular Flows, AIP Conference Proceedings Vol. 1227, 2010, pp. 240–260, ISBN: 978-0735407725.

Ribière P., Philippe P., Richard P., Delannay R., Bideau D., Slow compaction of granular systems, Journal of Physics: Condensed Matter, 17 (2005) S2743–S2754. https://doi.org/10.1088/0953-8984/17/24/024

Ribière Ph., Richard P., Philippe P., Bideau D., Delannay R., On the existence of stationary states during granular compaction, The European Physical Journal E, 22 (2007) 249–253. https://doi.org/10.1140/epje/e2007-00017-x

Sack A., Heckel M., Kollmer J.E., Zimber F., Pöschel T., Energy dissipation in driven granular matter in the absence of gravity, Physical Review Letters, 111 (2013) 018001. https://doi.org/10.1103/PhysRevLett.111.018001

Saint-Cyr B., Radjai F., Delenne J.-Y., Sornay P., Cohesive granular materials composed of nonconvex particles, Physical Review E, 87 (2013) 052207. https://doi.org/10.1103/PhysRevE.87.052207

Saker A., Cares-Pacheco M.-G., Marchal P., Falk V., Powders flowability assessment in granular compaction: What about the consistency of Hausner ratio?, Powder Technology, 354 (2019) 52–63. https://doi.org/10.1016/j.powtec.2019.05.032

Schulze D., Powders and Bulk Solids: Behavior, Characterization, Storage and Flow, Springer International Publishing, Cham, 2021, ISBN: 978-3030767198. https://doi.org/10.1007/978-3-030-76720-4

Sonzogni M. Vanson J.-M., Ioannidou K., Reynier Y., Martinet S., Radjai F., Dynamic compaction of cohesive granular materials: scaling behavior and bonding structures, Soft Matter, 20 (2024) 5296–5313. https://doi.org/10.1039/D3SM01116J

Suaza-Montalvo A., Cares-Pacheco M.G., Falk V., Time-dependent behaviour of industrial granular materials under vibration: modelling and phenomenology, Chemical Engineering Science, 271 (2023a) 118571. https://doi.org/10.1016/j.ces.2023.118571

Suaza-Montalvo A., Cares Pacheco M.-G., Falk V., Vidéos des phenomenes observés pendant la compaction de poudres. Partie de la thèse: étude expérimentale de la compaction par vibration des poudres industrielles: phénoménologie et intérêt, Université de Lorraine, Dorel data repository (2023b). https://doi.org/10.12763/VKDBAS

Terzioglu F., Rongong J.A., Lord C.E., Influence of particle sphericity on granular dampers operating in the bouncing bed motional phase, Journal of Sound and Vibration, 554 (2023) 117690. https://doi.org/10.1016/j.jsv.2023.117690

Wu M., Wang J., Prediction of 3D contact force chains using artificial neural networks, Engineering Geology, 296 (2022) 106444. https://doi.org/10.1016/j.enggeo.2021.106444

Zhao Y., Phalswal P., Shetty A., Ambrose R.P.K., Effects of powder vibration and time consolidation on soft and hard wheat flour properties, KONA Powder and Particle Journal, 38 (2021) 226–234. https://doi.org/10.14356/kona.2021007

Authors' Short Biographies

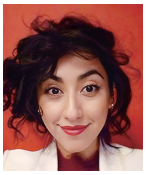

Dr. Maria-Graciela Cares is an Assistant Professor at the Université de Lorraine, affiliated with the Reactions and Chemical Engineering Laboratory (LRGP-CNRS), and teaches at the engineering school ENSIC in Nancy, France. She holds a degree in Physics Engineering from the University of Santiago de Chile, a Master's in Materials Science from the Université de Franche-Comté, and a Ph.D. from IMT Mines Albi. Her expertise spans Physics and Engineering, with a particular focus on granular physics and powder technologies, which has led to collaborations with the cosmetics, pharmaceutical, food, and automotive industries.

Prof. Véronique Falk graduated from École Nationale Supérieure des Industries Chimiques de Nancy (ENSIC), France, in 1991, earning degrees in Chemical Engineering and a Master's. She completed her PhD in 1995, focusing on catalytic cracking in collaboration with Total Raffinage. Since 2014, she has been a professor at Ecole Nationale Supérieure en Génie des Systèmes et de l'Innovation (Université de Lorraine), serving as deputy director since 2019. Her research at Laboratoire Réactions et Génie des Procédés (LRGP-CNRS) focuses on experimental powder technology, including rheology, mixing, granulation, compression, and product formulation, with extensive industry collaboration.